Enhanced vertical mixing associated with a nocturnal cold front passage and its impact on near-surface temperature and ozone concentration

Xiao-Ming Hu,[1] Petra M. Klein,[1,2] Ming Xue,[1,2] Alan Shapiro,[1,2] and Anita Nallapareddy[3]

Received 13 August 2012; revised 23 February 2013; accepted 27 February 2013; published 3 April 2013.

[1] A sudden rise in surface temperature is sometimes observed during the nighttime hours with the passage of cold fronts. The physics contributing to such nocturnal warming events and their potential impacts on atmospheric chemistry are not yet fully understood. In this study, a nocturnal warming event associated with a cold front passage in Oklahoma on 3 April 2006 is simulated with the Weather Research and Forecasting model with Chemistry (WRF/Chem). During the prefrontal period under clear-sky and calm conditions, surface radiative cooling resulted in a decoupled shallow surface layer in which air temperature and wind speed decreased quickly and ozone was removed efficiently by chemical reactions. During the passage of the cold front, strong wind shear enhanced turbulent mixing, which weakened the temperature inversion near the surface. Warmer and ozone-richer air from aloft was mixed downward to the surface. Thus, a sudden warming and nocturnal secondary ozone maxima were observed near the surface. Dry deposition of ozone at the surface was also enhanced in this warming event.

Citation: Hu, X.-M., P. M. Klein, M. Xue, A. Shapiro, and A. Nallapareddy (2013), Enhanced vertical mixing associated with a nocturnal cold front passage and its impact on near-surface temperature and ozone concentration, *J. Geophys. Res. Atmos.*, *118*, 2714–2728, doi:10.1002/jgrd.50309.

1. Introduction

[2] Previous studies have reported that a sudden rise in temperature can occur during the nighttime hours with the passage of a cold front [*Smith et al*., 1995; *Sanders and Kessler*, 1999; *Reeder et al*., 2000; *Beringer and Tapper*, 2000; *Doswell and Haugland*, 2007; *Shapiro et al*., 2009; *White*, 2009; *Nallapareddy et al*., 2011]. This phenomenon has been documented in Central Australia, Central U.S. (e.g., Oklahoma, Mississippi), and other regions [*Smith et al*., 1995; *White*, 2009; *Nallapareddy et al*., 2011]. During such warming events, the surface temperature typically rises by a few degrees Celsius (°C), but in extreme cases, it can rise by as much as 10°C [*Nallapareddy et al*., 2011]. Prior to nocturnal warming events, light winds (<3 m s^{-1}) often persist, which facilitates the development of a nocturnal temperature inversion (*Nallapareddy et al*., 2011). In a climatological study of warming events in Oklahoma, *Nallapareddy et al*. [2011] showed that the average increase in wind speed is larger during frontal passages associated with warming events than for non-warming cases. Such nocturnal warming events were speculated to be caused by the downward transport of warmer air by strong and gusty winds associated with the frontal passage [*Doswell and Haugland*, 2007; *Nallapareddy et al*., 2011]. However, other mechanisms (e.g., propagation of waves/bores on the nocturnal inversion surface) have also been suggested to be responsible for the downward transport of warmer air [*Clarke et al*., 1981; *Smith et al*., 1995; *White*, 2009; *Hartung et al*., 2010]. Additionally, several other questions regarding nocturnal warming events (e.g., their seasonal variation, factors affecting the magnitude of warming) remain to be understood. Detailed observational case studies and/or high-resolution numerical model simulations are needed to provide further insight [*Nallapareddy et al*., 2011].

[3] Understanding the physics and dynamics leading to these nocturnal warming events and accurately forecasting these events are significant for the energy management, transportation, and agriculture sectors [*White*, 2009; *Nallapareddy et al*., 2011]. For example, unresolved nocturnal warming events could result in inaccurate forecasts of daily minimum temperature. Daily minimum temperature plays critical roles in determining the occurrence of meteorological phenomena such as fog, frost, and freezing, all of which can be of great significance to transportation. Understanding nocturnal warming events may also have important implications for the parameterization of boundary layer processes in numerical models [*Derbyshire*, 1999] and the dispersion of pollutants such as carbon dioxides and ozone [*Weber and Kurzeja*, 1991; *Salmond*, 2005; *Acevedo et al*., 2006].

[1]Center for Analysis and Prediction of Storms, The University of Oklahoma, Norman, Oklahoma, USA.
[2]School of Meteorology, The University of Oklahoma, Norman, Oklahoma, USA.
[3]Weathernews Inc., Norman, Oklahoma, USA.

Corresponding author: X.-M. Hu, Center for Analysis and Prediction of Storms, The University of Oklahoma, Norman, OK 73072, USA. (xhu@ou.edu)

2169-897X/13/10.1002/jgrd.50309

[4] Inaccuracies exist in model simulations of dispersion of pollutants within the atmospheric boundary layer [*Neu*, 1995; *Seigneur*, 2001; *Hu et al*., 2012]. While much progress has been made in simulating dispersion of pollutants in the daytime convective boundary layer, more efforts are needed to improve the simulation of nighttime dispersion processes [*Solomon et al*., 2000; *Salmond and McKendry*, 2002, 2005; *Beare et al*., 2006; *Brown*, 2008; *Hong*, 2010; *Fernando and Weil*, 2010; *Hu et al*., 2010c, 2012, 2013]. In the traditional view of the diurnal variation of ozone in the atmospheric boundary layer, ozone is depleted in the shallow stable boundary layer and remains relatively invariant in the residual layer during nighttime. In the morning, the preserved residual layer ozone is mixed down to the surface where it can contribute to the buildup of ground-level ozone [*Zhang et al*., 1998; *Zhang and Rao*, 1999; *Neu et al*., 1994; *Aneja et al*., 2000; *Yorks et al*., 2009; *Morris et al*., 2010; *Tong et al*., 2011]. However, recent studies reported that under certain circumstances, the residual layer ozone can be effectively dispersed and its contribution to the ground-level ozone is reduced during the subsequent morning [*Hu et al*., 2012, 2013].

[5] During the summer months, elevated surface ozone concentrations are frequently observed near Tulsa and Oklahoma City, two major metropolitan areas of Oklahoma. Daytime peak values close to or even above 80 parts per billion by volume (ppbv) are quite typical, and during ozone episodes, elevated concentrations reaching 40 ppbv are often reported at night [*Kastner-Klein et al*., 2002; *Williams et al*., 2009; *Klein et al*., 2010]. Long-range transport and vertical mixing processes were identified as key processes contributing to ozone accumulation in Oklahoma [*Solomon et al*., 2000; *Hidy*, 2000; *Kastner-Klein et al*., 2002]. Vertical mixing processes associated with a cold front in the eastern U.S. have been shown to affect the surface ozone variation [*Hu et al*., 2012]. Since warming events associated with nocturnal cold front passages are likely also significant mixing events, a question arises as to whether such nocturnal warming events play an important role in reducing the residual layer ozone and altering the variation of surface ozone.

[6] Although nocturnal warming events associated with a cold front were investigated using surface meteorological observations in climatological and case studies [*Sanders and Kessler*, 1999; *Doswell and Haugland*, 2007; *White*, 2009; *Shapiro et al*., 2009; *Nallapareddy et al*., 2011], their detailed mechanisms, the spatial and temporal extent of the abrupt warming, and their implication for air pollution are not always clear. This motivates the further investigation of the spatial extent and vertical structure of wind, temperature, and ozone concentration in a cold front-associated nocturnal warming event using numerical simulations.

[7] In the study of *Nallapareddy et al*. [2011], a climatology of nocturnal warming events associated with cold fronts was created using 6 years of Oklahoma Mesonet [*McPherson et al*., 2007] data from 2003 to 2008. Nocturnal warming events associated with cold-frontal passages were found to occur frequently across Oklahoma. Of the cold fronts observed in this study, 91.5% produced at least one warming event at an Oklahoma Mesonet station. When normalized by the monthly number of cold-frontal passages, the winter months still had the most number of warming events and the warming events occurred most frequently between 2300 and 0200 UTC. Warming events were associated with weaker initial winds and stronger initial temperature inversions. Moreover, the nocturnal temperature inversion weakened more and the surface wind speeds increased more during the cold frontal passages that were associated with warming events. The results are consistent with previous studies that suggest the warming events are due to the "mixing out" of the nocturnal temperature inversion.

[8] In this study, a nocturnal warming event that occurred on the night of 2–3 April 2006 in Oklahoma is chosen for a detailed numerical simulation study using the Weather Research and Forecasting model with Chemistry (WRF/Chem) [*Grell et al*., 2005]. This event was among the six most widespread cold front-associated nocturnal warming events in Oklahoma from 2003 to 2008 as documented by *Nallapareddy et al*. [2011].

[9] The paper is organized as follows. Section 2 describes the numerical model set-up, the numerical simulations conducted, and the observational data used for evaluating the model. In section 3, the simulation results are presented and the physical processes that can explain the findings are discussed. Conclusions and further discussions are given in section 4.

2. Methods

2.1. Three-Dimensional Simulation

[10] To investigate the detailed mechanisms behind the nocturnal warming event associated with a cold front passage on 2–3 April 2006 in Oklahoma and its impacts on low-level ozone concentrations, a three-dimensional simulation was conducted with WRF/Chem version 3.2.1 [*Grell et al*., 2005]. Two 1-way nested domains (Figure 1) were employed with horizontal grid spacings of 22.5 and 4.5 km, respectively. Each domain had 48 vertical layers extending from the surface to 100 hPa. The sigma levels and mid-layer heights of the lowest 20 model layers are shown in Table 1. All model domains used the Dudhia shortwave radiation algorithm [*Dudhia*, 1989], the rapid radiative transfer model (*Mlawer et al*., 1997) for longwave radiation, the WRF Single-Moment 6-class Microphysics scheme [*Hong et al*., 2004], and the Noah land-surface scheme [*Chen and Dudhia*, 2001]. The radiation schemes were called every 30 min. Planetary boundary layer (PBL) parameterization schemes are relied upon to simulate boundary layer processes. Since the non-local Yonsei University (YSU) [*Hong et al*., 2006] PBL scheme performed well in simulating nighttime mechanically driven boundary layers [e.g., *Hu et al*., 2010a; *Hong*, 2010], it was chosen for the simulation reported in this study. The $1^\circ \times 1^\circ$ National Centers for Environmental Prediction Final Global Forecast System analyses were used for the initial and boundary conditions of all meteorological variables.

[11] To determine gas-phase chemical reactions, the Regional Atmospheric Chemistry Mechanism [*Stockwell et al*., 1997] was used. Hourly anthropogenic emissions of chemical species came from the 4 km × 4 km national emission inventory for the year 2005. Biogenic emissions were calculated using established algorithms [*Guenther et al*., 1994]. The focus of the modeling study is on the nocturnal warming event associated with the cold front observed in Oklahoma at around 0400 UTC (2200 local standard time;

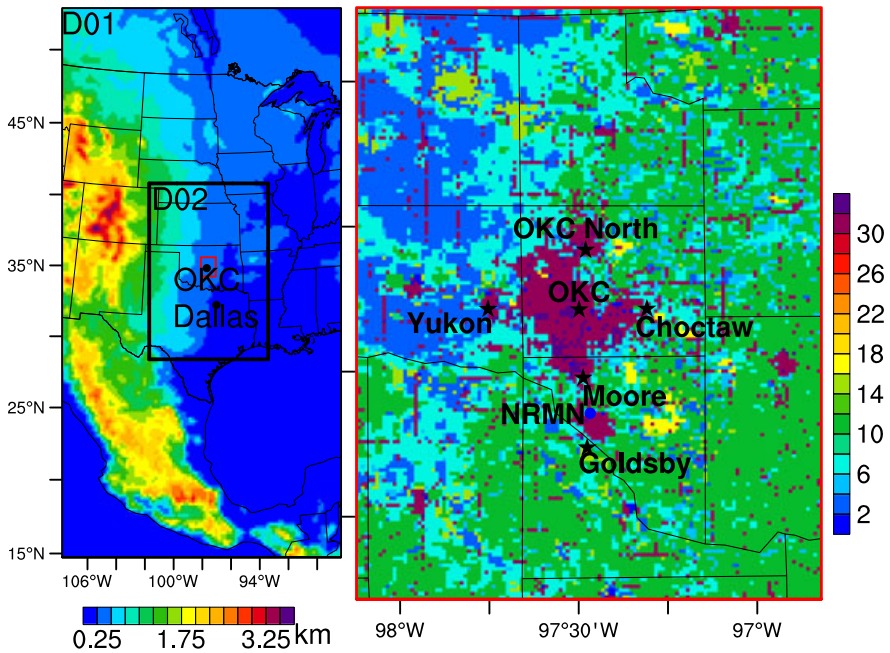

Figure 1. Map of model domains and terrain height (background color) used in this study is presented on the left. The land use categories in the red box around Oklahoma City (OKC) are zoomed in on the right. The locations of the six EPA sites in the Oklahoma City metropolitan area (i.e., Choctaw, Goldsby, Moore, OKC, OKC North, and Yukon) and the Norman Mesonet site (NRMN) are marked.

Table 1. Sigma Levels and Midlayer Heights (m agl) of the Lowest 20 Model Layers

Sigma levels	1.0	0.997	0.994	0.991	0.988	0.985	0.975	0.97	0.96	0.95
Midlayer heights	12	37	61	86	111	144	186	227	290	374
Sigma levels	0.94	0.93	0.92	0.91	0.895	0.88	0.865	0.85	0.825	0.8
Midlayer heights	459	545	631	717	826	958	1092	1226	1409	1640

LST) on 3 April 2006. To test the effect of different spin-up times, atmospheric simulations were initialized at 1200 UTC on 2 April, 1800 UTC on 2 April, and 0000 UTC on 3 April, respectively. The simulation initiated at 0000 UTC on 3 April showed the best overall performance based on the comparison with the surface observations from the Oklahoma Mesonet described below, and its results are thus presented in this paper. The simulations ended at 0000 UTC 4 August 2006. Boundary conditions for the chemical species were extracted from the output of the global model MOZART4 with a resolution of $2.8° \times 2.8°$ [*Emmons et al.*, 2010]. To allow for a longer spin-up time for chemical species, their initial conditions were extracted from the output of another WRF/Chem simulation initialized at 0000 UTC on 2 April with the MOZART4 output.

2.2. Data Sets for Model Evaluation

[12] Meteorological data collected by the Oklahoma Mesonet [*McPherson et al.*, 2007] and ozone data collected at the Environmental Protection Agency (EPA) Air Quality System (AQS) sites (available at http://www.epa.gov/ttn/airs/airsaqs/detaildata/downloadaqsdata.htm) were the primary data sources used to evaluate the model results in this study. As the average spacing between Mesonet stations is approximately 30 km, there is at least one station in each Oklahoma county [*Fiebrich and Crawford*, 2001]. In contrast, the EPA AQS sites have a much more inhomogeneous distribution. They are clustered near urban areas and are relatively sparse in rural areas. Data for meteorological variables from the Oklahoma Mesonet are reported every 5 min while hourly average ozone values are available for the AQS sites. The meteorological variables considered in this study included air temperature at 1.5 and 9 m above ground level (agl), dew point temperature at 1.5 m agl, and wind speed and direction at 10 m agl.

3. Results

[13] The nocturnal passage of the 2–3 April 2006 cold front across Oklahoma was associated with rapid temperature increases in a swath along the front [*Nallapareddy et al.*, 2011; *Shapiro et al.*, 2009]. Time series of observed meteorological variables on this day in Norman, Oklahoma, are displayed in Figures 2a and 2b. The warming event at Norman occurred at ~0400 UTC. During the evening hours preceding the rise in surface temperatures (0000–0400 UTC, i.e., 1800–2200 LST), wind speeds were light (Figure 2b) and skies were clear (figure not shown), providing conditions generally favorable for strong nocturnal radiative cooling in a thin boundary layer [*Acevedo and Fitzjarrald*, 2001; *Poulos et al.*, 2002]. During this period, the surface air cooled by ~2.5°C h^{-1} and moistened slightly. Strong surface radiative

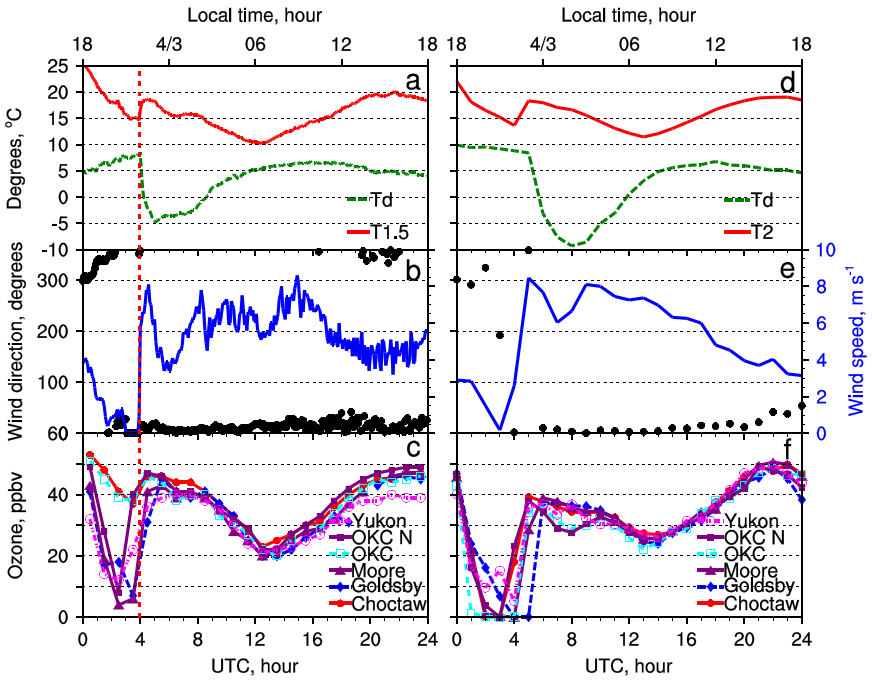

Figure 2. Observed and simulated time series of (a and d) temperature and dew point (Td), (b and e) wind speed and wind direction in Norman, and (c and f) ozone near the surface at the six EPA sites in central Oklahoma. Observed temperature is at 1.5 m while the simulated temperature is at 2 m agl. The onset of the nocturnal warming event is marked by the vertical red dashed line on the left column.

cooling can increase thermal stability near the surface, thus inhibiting turbulent motions. As a result, the surface layer may decouple from the free atmosphere above and the surface wind speeds reduce quickly. During the night of 2–3 April 2006, the winds had virtually died out before the arrival of the front (Figure 2b). These trends during the prefrontal period followed the typical characteristics of early evening surface-layer transitions under clear skies and calm conditions as reported in *Acevedo and Fitzjarrald* [2001]. The onset of the warming event at ~0400 UTC was characterized by a sudden increase in wind speed and temperature and a decrease in water vapor. Although the surface pressure rose on the night of 2–3 April, as is typical of a cold front passage, the rise was fairly gradual (not shown). Following the initial warming, the temperature decreased steadily throughout the remainder of the night, apparently due to further radiative cooling. These characteristics are typical of the cold front-associated nocturnal warming events documented in Oklahoma over a 6 year period [*Nallapareddy et al.*, 2011].

[14] Time series of hourly average ozone at six EPA AQS sites around Oklahoma City on this day is displayed in Figure 2c. During the night, ozone-generating photochemical reactions are shut down. While anthropogenic emissions of NO continue, surface ozone is normally depleted due to NO titration and dry deposition. Prior to the arrival of the cold front, hourly average ozone decreased to below 15 ppbv at Yukon, Moore, north Oklahoma City (OKC North), and Goldsby, while the decrease of ozone mixing ratios at central Oklahoma City (OKC) and Choctaw was not as substantial. The larger values of ozone at OKC and Choctaw may be due to two factors: first, heterogeneity of anthropogenic emissions may result in different chemical regimes across the OKC metro area [*Brown et al.*, 2007], and second, enhanced vertical mixing in the urban area due to a rougher surface and/or urban heat island effect may lead to stronger downward transport of ozone and enhanced surface ozone. Along with the onset of the warming event at ~0400 UTC, hourly ozone mixing ratios at the six sites increased during the passage of the cold front, resulting in nighttime ozone maxima with concentration values of 40–45 ppbv that are comparable to the afternoon peak concentrations recorded on the next day. While surface ozone maxima found in the afternoon are due to photochemical production [*Seinfeld and Pandis*, 1998], chemical production cannot explain the nighttime peaks. The observations thus support the hypothesis that the passage of the cold front played important roles in the formation of these nocturnal ozone maxima. Due to the lack of vertical concentration profiles and limited spatial coverage of the AQS monitoring network, further details about relevant processes can only be inferred by numerical simulations.

[15] The WRF/Chem simulation captured all of the important meteorological features of the event except the moistening of the surface air during the prefrontal period. Also, the drying of the surface air in the simulation lagged slightly behind the simulated occurrence of the warming (Figure 2). Possible errors in the initialization of the moisture (in both soil and atmosphere) could be causes of the discrepancies. The simulation initialized at 1800 UTC on 2 April performed better in terms of reproducing the moistening during the prefrontal period (not shown). The chemical simulation reproduced the nocturnal secondary ozone maximum associated with the warming event, with the predicted maximum values (~40 ppbv) being only slightly lower than the observed values (Figure 2f). In contrast to the observations, the simulated ozone concentration at OKC and Choctaw is

also depleted before the warming event. However, the 4 km resolution emission data used in the simulations are likely too coarse for cities with complex urban morphology. Particularly during the night, the chemical regimes within an urban area are typically highly variable in space [*Brown et al*., 2007]. Deficiencies in reproducing spatial patterns of emission and reaction rates with sufficient level of detail and/or underestimating vertical mixing related to the rougher urban surface and urban heat island effect may be partially responsible for the discrepancy.

[16] In addition to the features illustrated in the time series, the model captured the spatial distributions of meteorological variables associated with the nocturnal warming event. Figure 3 shows the simulated distributions of temperature at 2 m agl (T2), dew point at 2 m agl, and wind speed at 10 m agl at 0500 and 0600 UTC, 3 April 2006. The observed values from the Oklahoma Mesonet are overlaid for comparison. The spatial distribution of the warming swath along the cold front (which coincided with the leading edge of the strong northerly winds passing through Oklahoma) matches well with the Mesonet data (also consistent with *Nallapareddy et al*. [2011, Figure 4d]). The initial meteorological conditions at 0000 UTC do not have a warming swath present (not shown). Since horizontal advection cannot create the swath (it can only advect what is already there), some other processes must be responsible for the production of the swath. Both observation and simulation (Figures 3a and 3d) depict a weak synoptic-scale horizontal temperature gradient behind the leading momentum front. The result is consistent with the *Sanders and Kessler* [1999] finding that strong synoptic-scale surface temperature gradients were often associated with cold fronts with abrupt temperature decreases, while weak synoptic-scale temperature gradients were associated with temperature increases. Figures 3b and 3e show that there is a decrease of dew points behind the front in both the simulation and observations, but the simulation lags behind the observation. The position of the leading edge of the surge of wind speed in the simulation is in good agreement with observations (Figures 3c and 3f).

[17] Vertical mixing appears to play a critical role in the evolution of the nocturnal warming event. The simulated spatial distributions of the eddy diffusivity K for temperature in domain 2 at 0200, 0500, and 0800 UTC on 3 April 2006 are shown in Figure 4 to investigate in more detail the cause of the warming swath. The values of K are elevated behind the front, indicating enhanced vertical mixing. The leading

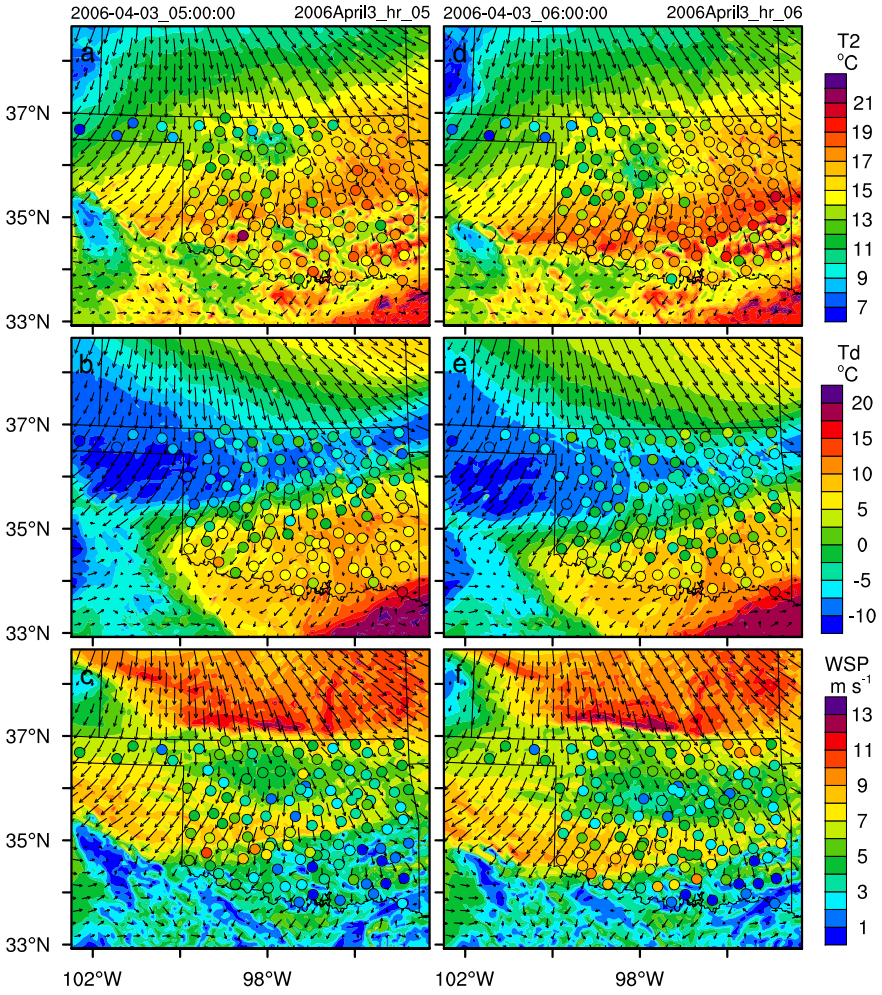

Figure 3. Simulated (a and d) 2 m temperature (T2), (b and e) 2 m dew point (Td), and (c and f) 10 m wind speed (WSP) at 0500 and 0600 UTC on 3 April 2006. Wind vectors show the simulated 10 m wind field. The observed values are indicated by shaded circles.

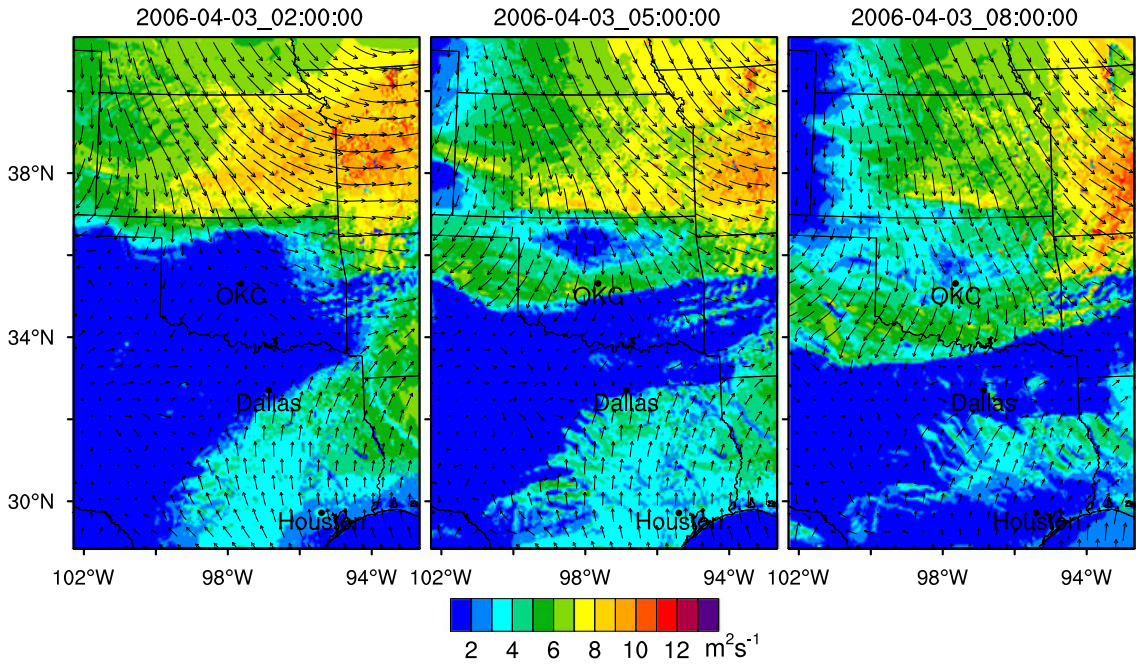

Figure 4. Simulated spatial distribution of eddy diffusivity for temperature near the surface at (left) 0200, (middle) 0500, and (right) 0800 UTC on 3 April 2006.

edge of the region with higher K matches well with the leading edge of higher T2 values (see, e.g., T2 at 0500 UTC in Figure 3a), which implies that the warming swath along the front was correlated with enhanced vertical mixing.

[18] Enhanced vertical mixing impacted the surface energy balances. The surface energy balances during cold front passage are of fundamental meteorological interest [*Beringer and Tapper*, 2000; *Steeneveld et al*., 2006]. Spatial distributions of sensible heat flux and soil heat flux simulated by the Noah land-surface model are displayed in Figure 5. Behind the cold front, upward soil heat flux was reduced to ~20 W m^{-2} and downward sensible heat flux was increased to as much as 100 W m^{-2}. Such trends in the surface energy exchanges are consistent with the observed trends associated with the cold-frontal passage in central Australia on 5 September 1996 [*Beringer and Tapper*, 2000]. Under the prefrontal conditions, upward soil heat flux dominated downward sensible heat flux to partially compensate the surface longwave radiative cooling, while behind the cold front, downward sensible heat flux played a dominant role in countering the surface radiative cooling.

[19] While enhanced vertical turbulent mixing near the front can significantly increase the surface temperature, horizontal advection near the front can also cause temperature changes. To understand their respective contributions, the instantaneous heating rates of air in the first model layer due to horizontal advection and vertical turbulent heat flux divergence are presented in Figure 6 for 0400 and 0500 UTC on 3 April 2006. The vertical heat flux divergence is computed as the difference between the surface sensible heat flux (from the land-surface model Noah) and the sensible heat flux at the interface of the first and second model layers due to vertical turbulence mixing. Using a first-order closure approach, the latter quantity can be calculated using the eddy diffusivity for temperature, K, and the vertical temperature gradient. As shown in Figure 6, vertical turbulent mixing plays a dominant role for heating in the narrow swath along the cold front, while horizontal advection also contributes to the increase of temperature at the very leading edge of the cold front, where cold, stably stratified air ahead of the front is replaced by air that is warmer due to the active mixing behind the front. The combined peak heating rates (which exceed 4°C h^{-1}) are in good agreement with the observed heating rates. Thus, the enhanced vertical mixing appears to be the root cause of surface temperature increase while horizontal advection of warmer, mixed air from behind the front also contributes to the local increase of surface temperature along the front. We also notice that ahead of the cold front, the spatial distributions of temperature and horizontal winds are quite inhomogeneous (Figure 3) presumably due to differences in the surface properties and localized intermittent turbulence in the stable boundary layer. As a result, the heating rate due to horizontal advection is also quite inhomogeneous without a discernible trend (Figure 6).

[20] Since this was a nocturnal event, the enhanced vertical mixing was unlikely driven by buoyancy. Instead, the very strong wind shear associated with the frontal passage likely induced turbulence and increased the vertical mixing. Vertical profiles of wind speed from the WRF/Chem simulation at Norman, OK, before and after the passage of the cold front are shown in Figure 7. Wind shear was substantially increased (by a factor of >2 near the surface) upon passage of the cold front. The YSU PBL scheme uses a K-profile method for vertical mixing in the stable boundary layer [*Hong and Pan*, 1996; *Hong et al*., 2006, 2010], in which K is formulated as a function of frictional velocity (u_*), boundary layer height (h), and the height from the surface (z):

$$K = k u_* \phi_m^{-1} Pr^{-1} z \left(1 - \frac{z}{h}\right)^p \quad (1)$$

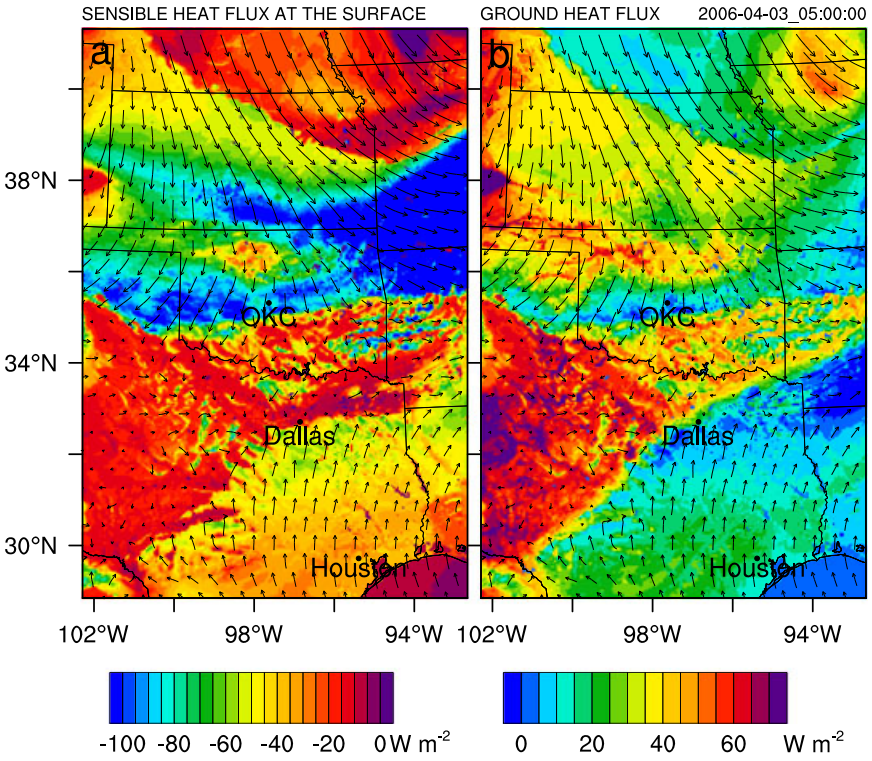

Figure 5. (a) Surface sensible heat flux and (b) soil heat flux at 0500 UTC on 3 April 2006 simulated by the Noah land-surface model in WRF/Chem. Note upward fluxes are positive for both sensible and soil heat fluxes in the figure.

where k is the von Karman constant (=0.4), ϕ_m is the dimensionless velocity gradient evaluated at the top of the surface layer, Pr is the Prandtl number, and p is the profile shape exponent taken to be 2. The boundary layer height has been defined in *Hong and Pan* [1996] and is proportional to the square of the wind speed at the top of the boundary layer and to the reciprocal of the temperature gradient. Stronger mechanical forcing associated with the passage of the cold front increased the surface frictional velocity (Figure 8a). The increased wind shear and reduced strength of the temperature inversion (shown later) behind the cold front increased the boundary layer height (Figure 8b). Additionally, ϕ_m decreases as stability weakens which together with the elevated frictional velocity and boundary layer height all contributed to an increase of K (Figure 4) according to (1).

[21] The enhanced vertical mixing associated with this warming event also affected the vertical redistribution of ozone. Figure 9 shows the simulated ozone at the surface and ~200 m agl over the study area. The model appeared to capture the features in the spatial distributions of ozone associated with this event. The leading edge of the increased surface ozone distribution matches well the leading edge of the wind surge and swath of warming shown in Figure 3. Ahead of the front, the spatial distribution of surface ozone is spotty because ozone was removed more efficiently by NO titration around anthropogenic emission sources such as big cities (e.g., Dallas and Houston, Texas) and major highways. Ozone behind the front was ubiquitously elevated at the surface (Figure 9a), while it was lower in the upper layers behind the front than ahead of the front (Figure 9b); clearly, downward mixing of ozone from aloft accompanying the cold front was responsible for the nighttime ozone maxima at surface sites (Figures 2c and 2f). Nighttime ozone maxima induced by intermittent turbulence have been reported in the presence of mesoscale motions such as low-level jets and breaking gravity waves [*Salmond and McKendry*, 2005; *Talbot et al*., 2005; *Hu et al*., 2012]. To our knowledge, our study is the first to document a nighttime ozone maximum induced by the passage of a cold front.

[22] Vertical potential temperature and ozone profiles before and after the passage of the cold front (Figure 10) further illustrate the impact of enhanced vertical mixing associated with the front. Before the passage of the front, i.e., at 0100–0400 UTC, there was a strong temperature inversion near the surface and the inversion strength increased with time due to surface radiative cooling, which indicated a strong thermodynamically stable and quiescent shallow boundary layer (less than 100 m deep; Figure 8b). At the same time, ozone also showed a strong gradient near the surface, which is consistent with observed nighttime ozone profiles over other urban areas [e.g., *Neu et al*., 1994; *Ding et al*., 2008; *Lin and McElroy*, 2010; *Ma et al*., 2012; *Hu et al*., 2012, 2013]. The ozone vertical gradient increased with time presumably because of efficient removal of ozone by NO titration (Figure 10b). Between 0100 and 0400 UTC, surface temperature decreased by ~6°C and surface O_3 decreased by ~22 ppbv (Figure 10), while above 100 m agl, neither temperature nor ozone changed much during this period. The nearly constant potential temperature and O_3 mixing ratios above 100 m agl indicate that the very cold and O_3-poor air near the surface was not being mixed upward to those levels during this period. Thus, those levels were isolated

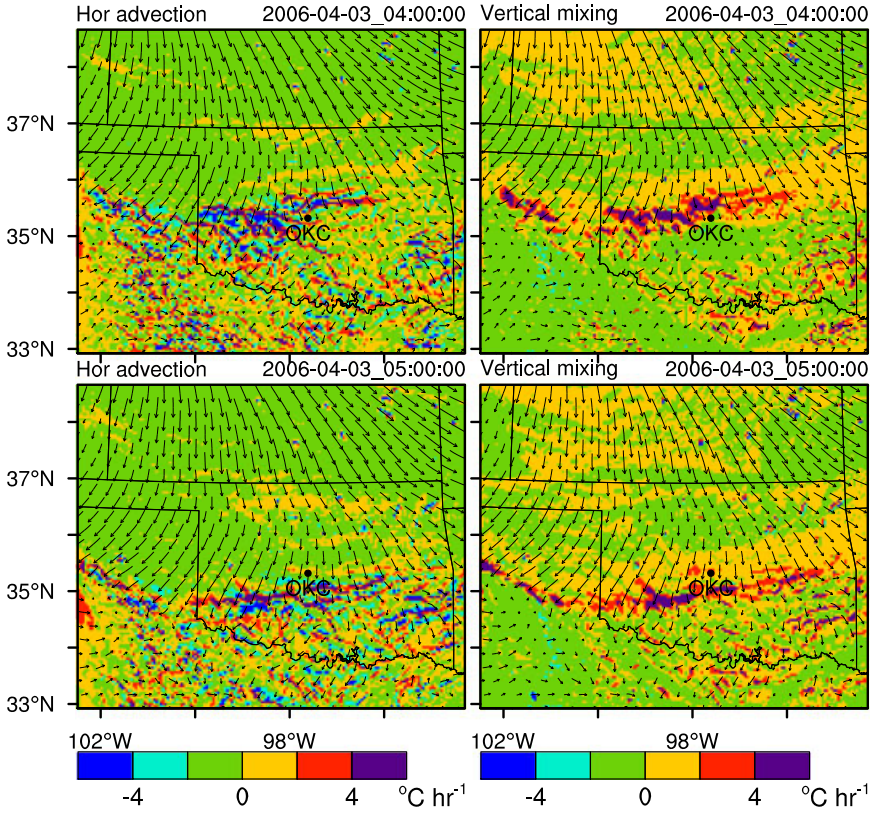

Figure 6. Heating rate of air in the first model layer due to horizontal advection and vertical heat flux divergence at (top row) 0400 and (bottom row) 0500 UTC on 3 April 2006. The vertical heat flux divergence is the difference between the surface sensible heat flux (Figure 5a) and the heat flux at the top of the first model layers due to vertical mixing. The latter is calculated using the eddy diffusivity and vertical temperature gradient between the first and second model layers.

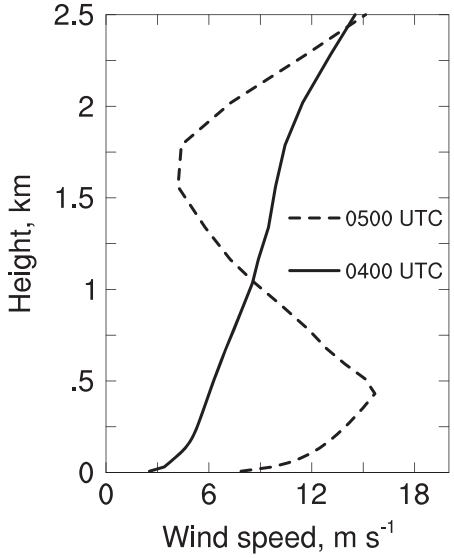

Figure 7. Simulated vertical profiles of wind speed at Norman, OK, before (0400 UTC) and after (0500 UTC) the passage of the cold front.

and detached from the shallow, very stable, boundary layer below [*Banta et al.*, 2007]. The light wind near the surface during the prefrontal period (Figures 2b and 2e) also suggests that the shallow stable boundary layer was decoupled from the residual layer above. Pollutants such as nitrogen oxides (NO_x) and carbon monoxide (CO), which are mostly emitted at the surface, have a reversed vertical gradient near the surface, i.e., they have the highest mixing ratios near the surface. During the prefrontal period, NO_x and CO accumulate within the shallow, decoupled stable boundary layer, while after the passage of the cold front, the mixing ratios of NO_x and CO near the surface decrease and those in the upper layers increase (figure not shown). In the case of potential temperature and ozone, for which positive, vertical gradients prevail ahead of the front, the values near the surface increase (by ~3°C and 30 ppbv, respectively) but decrease in the upper layers as the front passes (at 0500 UTC). In other words, the vertical gradients of those variables near the surface are all reduced after the passage of the cold front. The changes in the profiles of potential temperature and both passive and reactive pollutants are all consistent with the hypothesis that at and behind the cold front, stronger shear promotes vertical mixing which acts to reduce the vertical gradients of quasi-conservative variables. The boundary layer height behind the cold front is higher than 500 m in most areas (Figure 8b), supporting the notion of stronger coupling in the lower ~500 m agl nearly ubiquitously behind the cold front. While other mechanisms such as subsidence behind the cold front could, in principle, also contribute to the near-surface changes, the fact that near-surface vertical gradients decrease rather than increase suggests that vertical

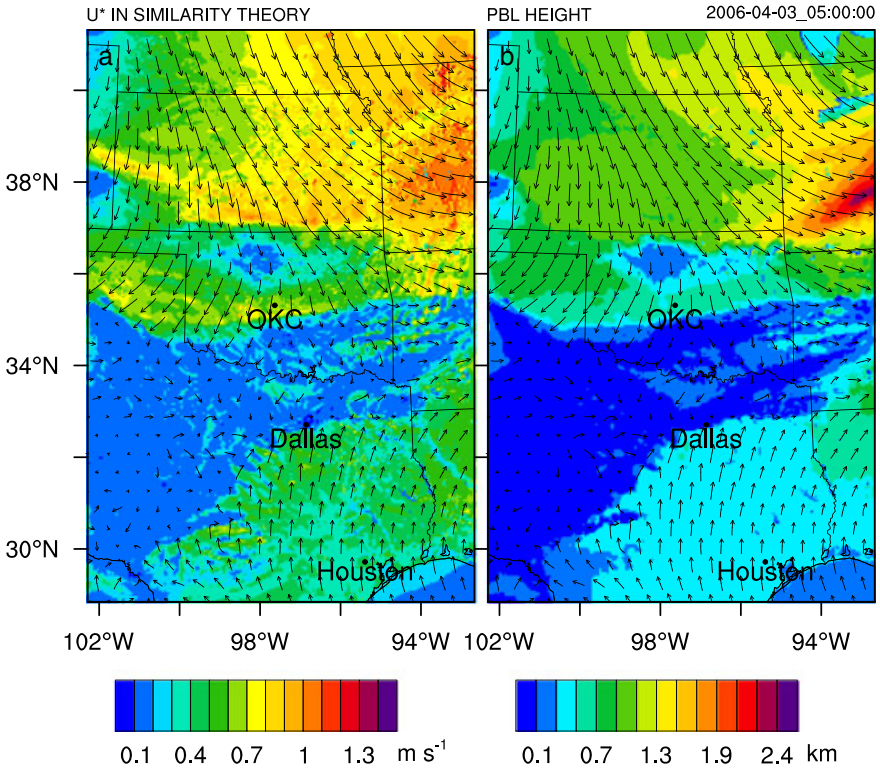

Figure 8. Simulated (a) surface frictional velocity (u_*) and (b) boundary layer height at 0500 UTC on 3 April 2006.

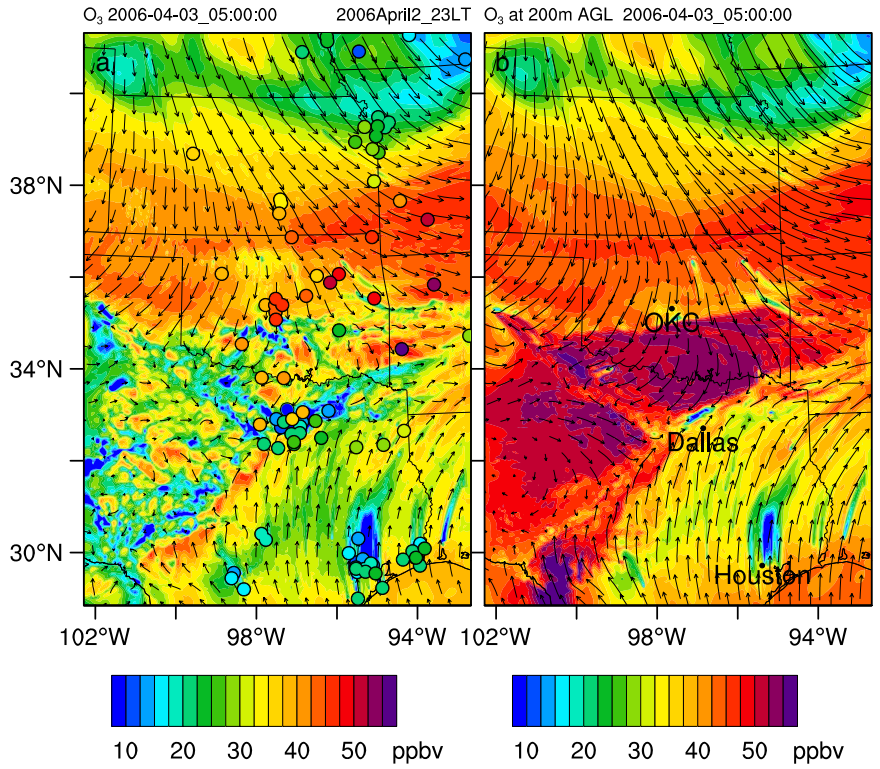

Figure 9. Simulated ozone mixing ratios at the (a) surface and (b) ~200 m agl at 0500 UTC on 3 April 2006. Shaded circles indicate ozone observations.

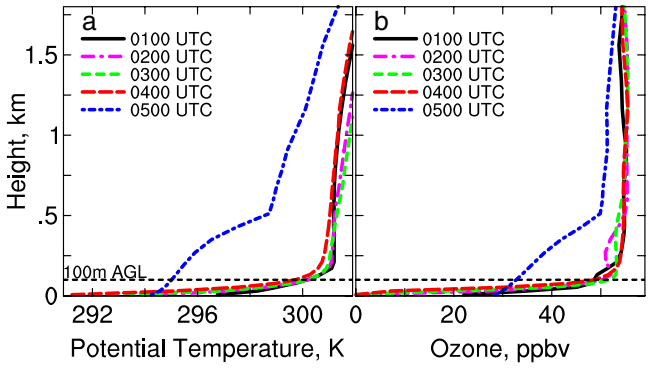

Figure 10. Simulated vertical profiles of (a) potential temperature and (b) ozone at Moore, OK, before (0100–0400 UTC) and after (0500 UTC) the passage of the cold front. The black dashed line marks the height of 100 m agl.

mixing is the dominant process since vertical advection associated with subsidence would actually enhance preexisting vertical gradients. Behind the frontal zone, the horizontal gradients are weak and the contribution of horizontal advection is weak (Figure 6).

[23] The spatial distribution of inversion strength $\left(\frac{dT}{dz}\right)$ near the surface further illustrates the impact of the cold front on the surface layer. As seen in Figure 11, the spatial pattern of the simulated inversion strength matches the observation quite well. The simulated inversion strength is calculated based on the simulated temperature at 2 m and the first model layer with a mid-layer height of ~12 m agl, while the observed values are calculated based on the observed temperature at 1.5 and 9 m agl. Thus, the simulated inversion strength may be weaker compared to observations since radiation cooling-induced temperature inversion is most

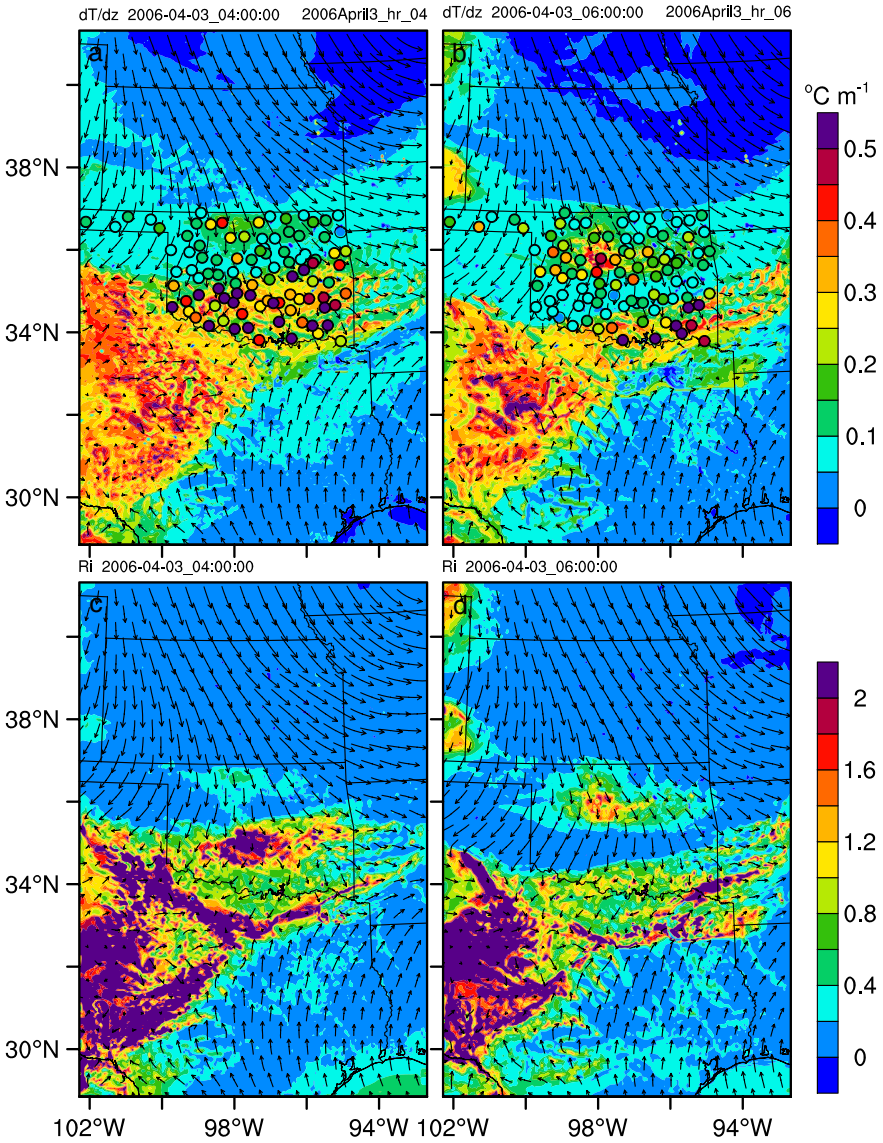

Figure 11. Simulated (a and b) temperature inversion strength $\left(\frac{dT}{dz}\right)$ and (c and d) Richardson number (Ri) near the surface at 0400 and 0600 UTC on 3 April 2006. The simulated temperature inversion strength is calculated based on the simulated temperature at 2 m and ~12 m agl. The observed values at Mesonet sites are indicated by shaded circles, which are calculated based on the observed temperature at 1.5 and 9 m agl.

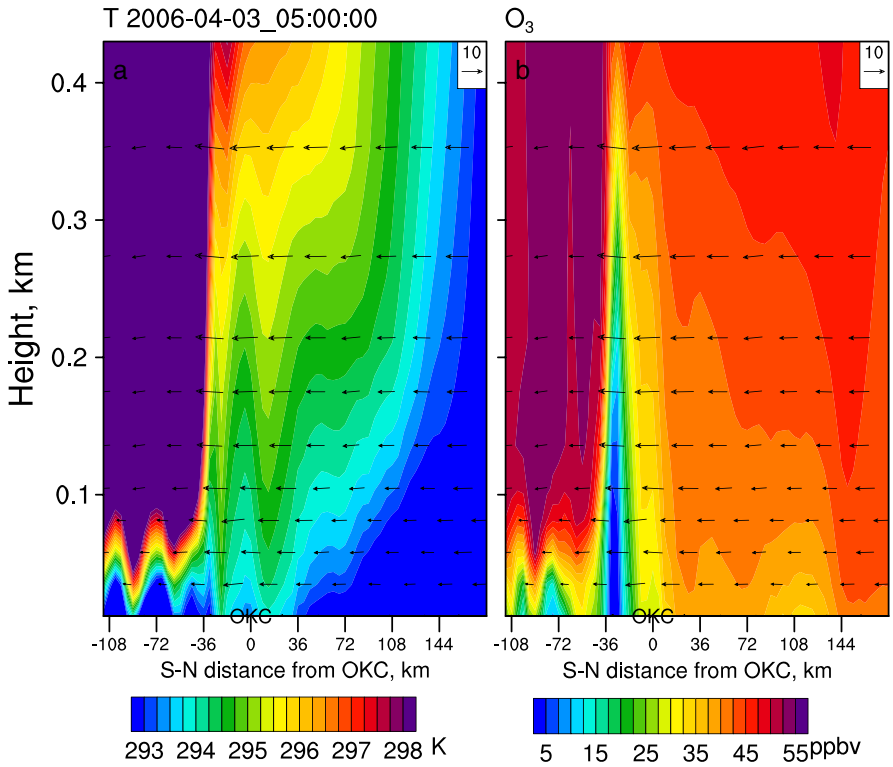

Figure 12. Simulated (a) potential temperature and (b) ozone at the south-north cross section passing through OKC.

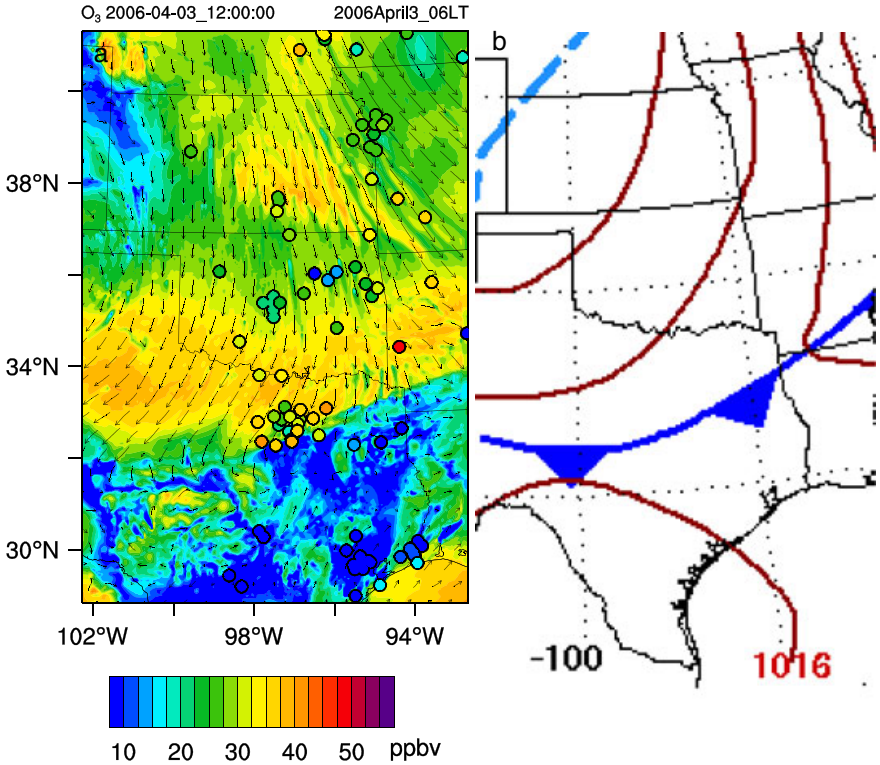

Figure 13. (a) Simulated ozone at 1200 UTC on 3 April 2006 and (b) surface weather map at the same time. The observed ozone values at the EPA AQS sites are overlaid with shaded circles. The surface weather map was prepared by the National Centers for Environmental Prediction, Hydrometeorological Prediction Center and archived at http://www.hpc.ncep.noaa.gov/dailywxmap/.

prominent near the surface. Ahead of the cold front, the observed inversion is as strong as 0.5°C m^{-1}. Such a strong stratification may lead to a collapse of turbulent mixing within a shallow surface layer that is decoupled from the upper warmer layers [*Derbyshire*, 1999; *Van De Wiel et al.*, 2002; *Delage et al.*, 2002; *Steeneveld et al.*, 2006]. The passage of the cold front reduced the strength of the inversion substantially. Significant weakening of nocturnal temperature inversions was found typical of the cold front-associated nocturnal warming events [*Nallapareddy et al.*, 2011]. The dynamic contrast across the front is also illustrated in the spatial distribution of Richardson number (*Ri*), an indicator of dynamic stability of a near-surface air layer, which is defined as

$$Ri = \frac{(g/T_v)\Delta\theta_v \Delta z}{(\Delta U)^2 + (\Delta V)^2} \quad (2)$$

where Δz is the height difference between the first and second model layers, and ΔU and ΔV are the respective changes in the U and V wind components over the Δz height interval. Smaller *Ri* often implies less stable conditions and higher levels of turbulence. Due to stronger wind shear and weaker inversion, the *Ri* behind the cold front is reduced to as low as <0.2 (Figures 11c and 11d). Such a weak stability generally suggests active turbulence [*Banta et al.*, 2003; *Galperin et al.*, 2007], which is consistent with the enhanced vertical mixing behind the cold front displayed in Figure 4.

[24] South-north vertical cross sections of potential temperature and ozone through Oklahoma City at 0500 UTC on 3 April 2006 are displayed in Figure 12. The cold front south of Oklahoma City is clearly illustrated by the significant vertical contrasts in temperature and ozone. Lower temperature followed the front leading edge in the layers above ~50m agl (Figure 12a). Behind the front leading edge, surface ozone is ubiquitously elevated while there is only a narrow swath (~60–70 km wide) with elevated temperature near the surface. Continuous radiative cooling and cold advection explain the gradual decrease of temperature at surface sites following the initial surge of temperature associated with the passage of the cold front (Figures 2a and 2d). Thus, vertical mixing, radiative cooling, and horizontal advection all played important roles in the variation of near-surface temperature within the domain.

[25] The nocturnal warming events associated with the cold front and its impact on ozone lasted until early the next morning. At 1200 UTC, the cold front passed Dallas, Texas with observed and simulated ozone mixing ratios around Dallas being elevated (Figure 13a). Overall, the simulated spatial distribution of surface ozone matches the observations at many of the EPA sites reasonably well, and the simulated leading edge of elevated ozone matches the cold front diagnosed from surface meteorological variables (Figure 13b).

[26] In addition to vertically redistributing ozone, enhanced turbulence associated with the cold front also affects the ozone dry deposition process. Dry deposition is a removal process of atmospheric material through turbulent transfer and uptake at the surface. It is an important regional and global sink for ozone [*Jacob and Wofsy*, 1990; *Sigler et al.*, 2002; *Saunois et al.*, 2009; *Hu et al.*, 2010b]. Enhanced turbulence associated with the cold front makes the transport of ozone down to the surface more effective, where ozone can adhere to it and be removed from the atmosphere. The total ozone dry deposition flux (F) is formulated as

$$F = -v_d \cdot C \quad (3)$$

where C represents the ozone mixing ratios near the surface. The proportionality factor v_d, which has units of length per unit time, is known as the dry deposition velocity. The ozone dry deposition velocity in the WRF/Chem model is parameterized using the method of *Wesley* [1989], in which v_d is the reciprocal of the total resistance (i.e., the sum of the aerodynamic resistance r_a, the quasi-laminar layer resistance r_b, and the surface/canopy resistance r_c):

$$v_d = 1/(r_a + r_b + r_c) \quad (4)$$

[27] The estimation of r_a and r_b involves frictional velocity (u_*) with a larger/smaller u_* leading to a smaller/larger resistance, and thus a larger/smaller deposition velocity. Since u_* was elevated behind the cold front (Figure 8a), v_d was correspondingly elevated (by 0.4–0.5 cm s^{-1}; Figure 14). The passage of the cold front enhanced both C (Figure 9) and v_d (Figure 14), thus increasing the total amount of ozone removed through dry deposition. Previous studies [*Hu et al.*, 2013] have shown that increased ozone dry deposition at night can reduce the boundary layer ozone concentration on the subsequent day.

[28] As illustrated in Figure 2, the WRF/Chem model reasonably reproduced the impacts of the nocturnal cold-frontal

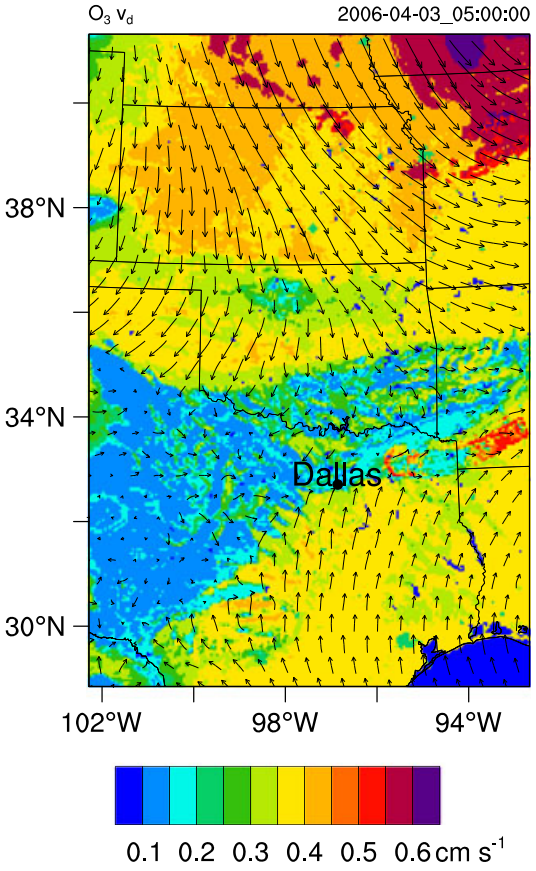

Figure 14. Simulated ozone dry deposition velocity at 0500 UTC on 3 April 2006.

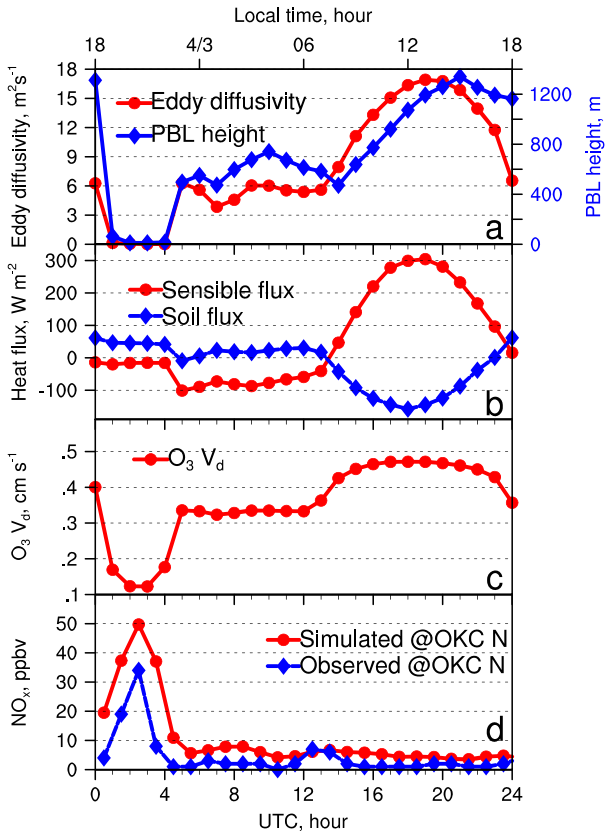

Figure 15. Simulated time series of (a) eddy diffusivity for temperature and boundary layer height, (b) sensible heat flux and soil heat flux, (c) O_3 dry deposition velocity in Norman, Oklahoma, and (d) simulated and observed NO_x at the OKC North EPA site.

passage on the time variation of meteorological variables (i.e., temperature, dew point, and wind) and O_3 near the surface. The simulated impacts of the cold-frontal passage on the variation of other variables are summarized in Figure 15. As analyzed in the previous paragraphs, due to the passage of the cold front, vigorous turbulence is triggered in a deeper boundary layer (Figure 15a). As a result, downward sensible heat flux is enhanced, upward soil heat flux is reduced (Figure 15b), surface O_3 dry deposition velocity is elevated (Figure 15c), vertical gradients of both meteorological variables and chemical species in the stable boundary layer are reduced, and the abundance of directly emitted pollutants is reduced near the surface (e.g., NO_x; Figure 15d). The observation at an EPA site (i.e., OKC North) confirmed the reduction of surface NO_x after the passage of the cold front (Figure 15d).

4. Conclusions and Discussions

[29] Previous studies of nocturnal warming events associated with cold-frontal passages were mostly based on observations from surface meteorological networks. However, many issues related to those events, e.g., spatial and temporal extent, impact on dispersion of pollutants, detailed mechanisms, were not fully understood. To investigate these issues, the nocturnal warming event in Oklahoma on 2–3 April 2006 was simulated with WRF/Chem in this study. Before the cold front passed through, radiative cooling at the surface resulted in a decoupled shallow surface layer under clear-sky and calm conditions. Surface temperature and wind speed decreased quickly during the prefrontal period. Ozone near the surface was removed efficiently around major anthropogenic emission sources due to NO titration. With the passage of the cold front, turbulence was induced by strong wind shear and mixed the warmer and ozone-richer air down to the surface from upper parts of the PBL. Thus, a sudden increase in near-surface temperature and ozone occurred with the passage of the front. The front-associated mixing produced a swath of warm air at the surface approximately 60–70 km wide just behind the leading edge of the strong and gusty winds (momentum front). Horizontal advection of the warm swath also contributed to the temperature increase at the leading edge of the cold front; however, the ultimate source of the warming was mixing since horizontal advection can advect but not create a thermal disturbance. Meanwhile, surface sensible heat flux was clearly increased behind the cold front, and this downward heat flux compensated the surface radiative cooling to the land surface. Ozone dry deposition velocity was also enhanced due to enhanced turbulence behind the cold front. More ozone would be removed at the surface as a result. Because of cold air advection and further radiative cooling, surface temperature decreased with time after passage of the warm swath. However, for ozone, a strong horizontal gradient was lacking following the front; thus, its mixing ratio was elevated in a wider area. This nocturnal warming event extended across several states and lasted for a few hours.

[30] Though not shown here, we also examined meteorological and chemical data for other cold-frontal passage cases identified in *Nallapareddy et al.* [2011] for both warming and non-warming cases. For most cold front passages with weak prefrontal winds, a concurrent enhancement of surface ozone was found in the AQS data. In many cases, sudden nocturnal increases in ozone were noted during frontal passage. For the cold-frontal passages with stronger prefrontal winds and weaker initial temperature inversions, the warming was less prominent. In such cases, the initial surface ozone did not appear to be efficiently removed and the changes of ozone associated with such cold-frontal passages were less prominent. Thus, it appears that weak initial winds and strong initial temperature inversions during the prefrontal period favors the occurrence of nocturnal warming events and the concurrent enhancement of surface ozone.

[31] **Acknowledgments.** This work was supported by funding from the Office of the Vice President for Research at The University of Oklahoma. The second author was also supported through the NSF Career award ILREUM (NSF ATM 0547882). The third author was also supported by NSF grants OCI-0905040, AGS-0802888, AGS-0750790, AGS-0941491, AGS-1046171, and AGS-1046081. Computations were performed at the Texas Advanced Computing Center (TACC). Three anonymous reviewers provided helpful comments that improved the paper.

References

Acevedo, O. C., and D. R. Fitzjarrald (2001), The early evening surface-layer transition: Temporal and spatial variability, *J. Atmos. Sci.*, *58*, 2650–2667.

Acevedo, O., O. L. L. Moraes, G. A. Degrazia, and L. E. Medeiros (2006), Intermittency and the exchange of scalars in the nocturnal surface layer, *Bound.-Layer Meteor.*, *119*, 41–55, doi:10.1007/s10546-005-9019-3.

Aneja, V. P., R. Mathur, S. P. Arya, Y. Li, G. C. Murray, and T. L. Manuszak (2000), Coupling the vertical distribution of ozone in the atmospheric boundary layer, *Environ. Sci. Technol.*, *34*, 2324–2329.

Banta, R. M., Y. L. Pichugina, and R. K. Newsom (2003), Relationship between low-level jet properties and turbulence kinetic energy in the nocturnal stable boundary layer, *J. Atmos. Sci.*, *60*, 2549–2555, doi:10.1175/1520-0469(2003)060<2549:RBLJPA>2.0.CO;2.

Banta, R. M., L. Mahrt, D. Vickers, J. Sun, B. B. Balsley, Y. L. Pichugina, and E. J. Williams (2007), The very stable boundary layer on nights with weak low-level jets, *J. Atmos. Sci.*, *64*, 3068–3090, doi:10.1175/JAS4002.1.

Beare, R. J., et al. (2006), An intercomparison of large-eddy simulations of the stable boundary layer, *Bound.-Layer Meteor.*, *118*(2), 247–272, doi:10.1007/s10546-004-2820-6.

Brown, A. R. (2008), Upgrades to the boundary-layer scheme in the Met Office numerical weather prediction model, *Bound.-Layer Meteor.*, *128*, 117–132, doi:10.1007/s10546-008-9275-0.

Beringer, J., and N. J. Tapper (2000), The influence of subtropical cold fronts on the surface energy balance of a semi-arid station, *J. Arid Environ.*, *44*, 437–450.

Brown, S. S., W. P. Dube, H. D. Osthoff, D. E. Wolfe, W. M. Angevine, and A. R. Ravishankara (2007), High resolution vertical distributions of NO_3 and N_2O_5 through the nocturnal boundary layer, *Atmos. Chem. Phys.*, *7*, 139–149, doi:10.5194/acp-7-139-2007.

Chen, F., and J. Dudhia (2001), Coupling an advanced land surface hydrology model with the Penn State–NCAR MM5 Modeling System. Part I: Model implementation and sensitivity, *Mon. Wea. Rev.*, *129*, 569–585.

Clarke, R. H., R. K. Smith, and D. G. Reid (1981), The Morning Glory of the Gulf of Carpentaria: An atmospheric undular bore, *Mon. Wea. Rev.*, *109*, 1726–1750.

Delage, Y., P. Bartlett, and J. H. McCaughey (2002), Study of "soft" night-time surface-layer decoupling over forest canopies in a land surface model, *Bound.-Layer Meteor.*, *103*, 253–276, doi:10.1023/A:1017443021557.

Derbyshire, S. (1999), Boundary-layer decoupling over cold surfaces as a physical boundary-instability, *Bound.-Layer Meteor.*, *90*, 297–325.

Ding, A. J., T. Wang, V. Thouret, J. P. Cammas, and P. Nédélec (2008), Tropospheric ozone climatology over Beijing: Analysis of aircraft data from the MOZAIC program, *Atmos. Chem. Phys.*, *8*(1), 1–13, doi:10.5194/acp-8-1-2008.

Doswell, C. A., and M. J. Haugland (2007), A comparison of two cold fronts—Effects of the planetary boundary layer on the mesoscale, *Electron. J. Severe Storms Meteor.*, *2*, 1–12.

Dudhia, J. (1989), Numerical study of convection observed during the winter monsoon experiment using a mesoscale two-dimensional model, *J. Atmos. Sci.*, *46*, 3077–3107.

Emmons, L. K., et al. (2010), Description and evaluation of the Model for Ozone and Related Chemical Tracers, version 4 (MOZART-4), *Geoscientific Model Development*, *3*, 43–67, doi:10.5194/gmdd-2-1157-2009.

Fernando, H. J. S., and J. C. Weil (2010), Whither the stable boundary layer?, *Bull. Amer. Meteor. Soc.*, *91*, 1475–1484, doi:10.1175/2010BAMS2770.1.

Fiebrich, C. A., and K. C. Crawford (2001), The impact of unique meteorological phenomena detected by the Oklahoma Mesonet and ARS Micronet on automated quality control, *Bull. Amer. Meteor. Soc.*, *82*, 2173–2187.

Galperin, B., S. Sukoriansky, and P. S. Anderson (2007), On the critical Richardson number in stably stratified turbulence, *Atmos. Res. Lett.*, *8*, 65–69, doi:10.1002/asl.153.

Grell, G. A., S. E. Peckham, R. Schmitz, S. A. McKeen, G. Frost, W. C. Skamarock, and B. Eder (2005), Fully coupled online chemistry within the WRF model, *Atmos. Environ.*, *39*, 6957–6975, doi:10.1016/j.atmosenv.2005.04.027.

Guenther, A., P. Zimmerman, and M. Wildermuth (1994), Natural volatile organic compound emission rate estimates for U.S. woodland landscapes, *Atmos. Environ.*, *28*, 1197–1210.

Hartung, D. C., J. A. Otkin, J. E. Martin, and D. D. Turner (2010), The life cycle of an undular bore and its interaction with a shallow, intense cold front, *Mon. Wea. Rev.*, *138*, 886–908, doi:10.1175/2009MWR3028.1.

Hidy G. M. (2000), Ozone process insights from field experiments part I: Overview, *Atmos. Environ.*, *34*, 2001–2022.

Hong, S.-Y., and H.-L. Pan (1996), Nonlocal boundary layer vertical diffusion in a medium-range forecast model, *Mon. Wea. Rev.*, *124*, 2322–2339.

Hong, S.-Y., J. Dudhia, and S.-H. Chen (2004), A revised approach to ice microphysical processes for the bulk parameterization of cloud and precipitation, *Mon. Wea. Rev.*, *132*, 103–120, doi:10.1175/1520-0493(2004)132<0103:ARATIM>2.0.CO;2.

Hong, S.-Y., Y. Noh, and J. Dudhia (2006), A new vertical diffusion package with explicit treatment of entrainment processes, *Mon. Wea. Rev.*, *134*, 2318–2341, doi:10.1175/MWR3199.1.

Hong S-Y. (2010), A new stable boundary-layer mixing scheme and its impact on the simulated East Asian summer monsoon, *Q. J. R. Meteorol. Soc.*, *136*, 1481–1496, doi:10.1002/qj.665.

Hu, X.-M., J. W. Nielsen-Gammon, and F. Zhang (2010a), Evaluation of three planetary boundary layer schemes in the WRF model, *J. Appl. Meteor. Climatol.*, *49*, 1831–1844, doi:10.1175/2010JAMC2432.1.

Hu, X.-M., J. D. Fuentes, and F. Zhang (2010b), Downward transport and modification of tropospheric ozone through moist convection, *J. Atmos. Chem.*, *65*, 13–35, doi:10.1007/s10874-010-9179-5.

Hu, X.-M., F. Zhang, and J. W. Nielsen-Gammon (2010c), Ensemble-based simultaneous state and parameter estimation for treatment of mesoscale model error: A real-data study, *Geophys. Res. Lett.*, *37*, L08802, doi:10.1029/2010GL043017.

Hu, X.-M., D. Doughty, K. J. Sanchez, E. Joseph, and J. D. Fuentes (2012), Ozone variability in the atmospheric boundary layer in Maryland and its implications for vertical transport model, *Atmos. Environ.*, *46*, 354–364, doi:10.1016/j.atmosenv.2011.09.054.

Hu, X.-M., P. Klein, M. Xue, F. Zhang, D. C. Doughty, R. Forkel, E. Joseph, and J. D. Fuentes (2013), Impact of the vertical mixing induced by low-level jets on boundary layer ozone concentration, *Atmos. Environ.*, *70*, 123–130, doi:10.1016/j.atmosenv.2012.12.046.

Jacob, D. J., and S. C. Wofsy (1990), Budgets of reactive nitrogen, hydrocarbons, and ozone over the Amazon forest during the wet season, *J. Geophys. Res.*, *95*, 16,737–16,754.

Kastner-Klein, P. M., D. Williams, and F. Hall (2002), Long-range transport of ozone pollution to Oklahoma City, *Bull. Amer. Meteor. Soc.*, *83*(5), 666–666.

Klein, P. M., J. K. Lundquist, and J. B. Basara (2010), Mixing processes in the nocturnal atmospheric boundary layer and their impacts on urban ozone concentrations and heat island intensity, Proceedings of the 19th Symposium on Boundary Layers and Turbulence, 1-6 August 2010, Keystone, CO, USA.

Lin, J. T., and M. B. McElroy (2010), Impacts of boundary layer mixing on pollutant vertical profiles in the lower troposphere: Implications to satellite remote sensing, *Atmos. Environ.*, *44*(14), 1726–1739, doi:10.1016/j.atmosenv.2010.02.009.

Ma, Z., H. Xu, W. Meng, X. Zhang, J. Xu, Q. Liu, and Y. Wang (2012), Vertical ozone characteristics in urban boundary layer in Beijing, *Environ. Monit. Assess.*, doi:10.1007/s10661-012-2958-5.

McPherson, R. A., et al. (2007), Statewide monitoring of the mesoscale environment: A technical update on the Oklahoma Mesonet, *J. Atmos. Oceanic Technol.*, *24*, 301–321, doi:doi:10.1175/JTECH1976.1.

Mlawer, E. J., S. J. Taubman, P. D. Brown, M. J. Iacono, and S. A. Clough (1997), Radiative transfer for inhomogeneous atmospheres: RRTM, a validated correlated-k model for the longwave, *J. Geophys. Res.*, *102D*, 16 663–16 682.

Morris, G. A., B. Ford, B. Rappengluck, A. M. Thompson, A. Mefferd, F. Ngan, and B. Lefer. (2010), An evaluation of the interaction of morning residual layer and afternoon mixed layer ozone in Houston using ozonesonde data, *Atmos. Environ.*, *44*, 4024–4034, doi:10.1016/j.atmosenv.2009.06.057.

Nallapareddy, A., A. Shapiro, and J. J. Gourley (2011), A climatology of nocturnal warming events associated with cold-frontal passages in Oklahoma, *J. Appl. Meteor. Climatol.*, *50*, 2042–2061, doi:10.1175/JAMC-D-11-020.1.

Neu, U., T. Kunzle, and H. Wanner (1994), On the relation between ozone storage in the residual layer and the daily variation in near surface ozone concentration—A case study, *Bound.-Layer Meteor.*, *69*, 221–247.

Neu, U. (1995), A parameterization of the nocturnal ozone reduction in the residual layer by vertical downward mixing during summer smog situations using sodar data, *Bound.-Layer Meteor.*, *73*, 189–193.

Poulos, G. S., et al. (2002), CASES-99: A comprehensive investigation of the stable nocturnal boundary layer, *Bull. Amer. Meteor. Soc.*, *83*, 555–581, doi:10.1175/1520-0477(2002)083<0555:CACIOT>2.3.CO;2.

Reeder, M. J., R. K. Smith, R. Deslandes, N. J. Tapper, and G. A. Mills (2000), Subtropical fronts observed during the 1996 Central Australian Fronts Experiment, *Aust. Meteor. Mag.*, *49*, 181–200.

Salmond, J. A. (2005), Wavelet analysis of intermittent turbulence in a very stable nocturnal boundary layer: Implications for the vertical mixing of ozone, *Bound.-Layer Meteor.*, *114*(3), 463–488, doi:10.1007/s10546-004-2422-3.

Salmond, J. A., and I. G. McKendry (2002), Secondary ozone maxima in a very stable nocturnal boundary layer: Observations from the Lower Fraser Valley, B.C., *Atmos. Environ.*, *36*, 5771–5782, doi:10.1016/S1352-2310(02)00698-2.

Salmond, J. A., and I. G. McKendry (2005), A review of turbulence in the very stable boundary layer and its implications for air quality, *Progress Phys. Geography*, *29*, 171–188, doi:10.1191/0309133305pp442ra.

Sanders, F., and E. Kessler (1999), Frontal analysis in the light of abrupt temperature changes in a shallow valley, *Mon. Wea. Rev.*, *127*, 1125–1133.

Saunois, M., C. E. Reeves, C. H. Mari, J. G. Murphy, D. J. Stewart, G. P. Mills, D. E. Oram, and R. M. Purvis (2009), Factors controlling the distribution of ozone in the West African lower troposphere during the AMMA (African Monsoon Multidisciplinary Analysis) wet season campaign, *Atmos. Chem. Phys.*, *9*, 6135–6155, doi:10.5194/acp-9-6135-2009.

Seigneur, C. (2001), Current status of air quality modeling for particulate matter, *J. Air Waste Manage. Assoc.*, *51*, 1508–1821.

Seinfeld, J. H., and S. N. Pandis (1998), Atmospheric Chemistry and Physics: From Air Pollution to Climate Change, John Wiley, New York, 1326 p.

Shapiro, A., P. M. Klein, S. C. Arms, D. Bodine, and M. Carney (2009), The Lake Thunderbird Micronet Project, *Bull. Amer. Meteor. Soc.*, *90*, 811–823, doi:10.1175/2008BAMS2727.1.

Sigler, J. M., J. D. Fuentes, R. C. Heitz, M. Garstang, and G. Fisch (2002), Ozone dynamics and deposition processes at a deforested site in the Amazon basin, *Ambio*, *3*, 21–28, doi:10.1579/0044-7447-31.1.21.

Smith, R. K., M. J. Reeder, N. J. Tapper, and D. R. Christie (1995), Central Australian cold fronts, *Mon. Wea. Rev.*, *123*, 16–38.

Solomon, P., E. Cowling, G. Hidy, and C. Furiness (2000), Comparison of scientific findings from major ozone field studies in North America and Europe, *Atmos. Environ.*, *34*, 1885–1920.

Steeneveld, G. J., B. J. H. van de Wiel, and A. A. M. Holtslag (2006), Modeling the arctic stable boundary layer and its coupling to the surface, *Bound.-Layer Meteor.*, *118*, 357–378, doi:10.1007/s10546-005-7771-z.

Stockwell, W. R., F. Kirchner, M. Kuhn, and S. Seefeld (1997), A new mechanism for regional atmospheric chemistry modeling, *J. Geophys. Res.*, *102*, 25 847–25 879.

Talbot, R., H. Mao, and B. Sive (2005), Diurnal characteristics of surface level O_3 and other important trace gases in New England, *J. Geophys. Res.*, *110*, D09307, doi:10.1029/2004JD005449.

Tong, N. Y. O., D. Y. C. Leung, and C. H. Liu (2011), A review on ozone evolution and its relationship with boundary layer characteristics in urban environments, *Water Air Soil Pollut.*, *214*, 13–36, doi:10.1007/s11270-010-0438-5.

Van de Wiel, B. J. H., R. J. Ronda, A. F. Moene, H. A. R. De Bruin, and A. A. M. Holtslag (2002), Intermittent turbulence and oscillations in the stable boundary layer over land. Part I: A bulk model, *J. Atmos. Sci.*, *59*, 942–958, doi:10.1175/1520-0469(2002)059<0942:ITAOIT>2.0.CO;2.

Weber, A. H., and R. J. Kurzeja (1991), Nocturnal planetary boundary layer structure and turbulence episodes during the Project STABLE field program, *J. Appl. Meteor.*, *30*, 1117–1133.

Wesley, M. L. (1989), Parameterization of surface resistance to gaseous dry deposition in regional numerical models, *Atmos. Environ.*, *16*, 1293–1304.

White, L. D. (2009), Sudden nocturnal warming events in Mississippi, *J. Appl. Meteor. Climatol.*, *48*, 758–775, doi:10.1175/2008JAMC1971.1.

Williams, D. J., W. T. Potter, W. W. Clarkson, D. A. Sanders, and J. E. Stevens (2009), The impact of background ozone on compliance with Revised National Ambient Air Quality Standards, *J. Air Waste Manage. Assoc.*, *59*(1), 52–57, doi:10.3155/1047-3289.59.1.52.

Yorks, J. E., A. M. Thompson, E. Joseph, and S. K. Miller (2009), The variability of free tropospheric ozone over Beltsville, Maryland (39N, 77W) in the summers 2004–2007, *Atmos. Environ.*, *43*, 1827–1838, doi:10.1016/j.atmosenv.2008.12.049.

Zhang, J., and S. T. Rao (1999), The role of vertical mixing in the temporal evolution of ground-level ozone concentrations, *J. Appl. Meteor.*, *38*, 1674–1691.

Zhang, J., S. T. Rao, and S. M. Daggupaty (1998), Meteorological processes and ozone exceedances in the Northeastern United States during the 12–16 July 1995 episode, *J. Appl. Meteor.*, *37*, 776–789.